

Intercomparison of Convective-Aggregation States with two Cloud Resolving Models

Paolina Bongioannini Cerlini¹, Miriam Saraceni¹, and Lorenzo Silvestri¹

¹University of Perugia

November 26, 2022

Abstract

The Radiative-Convective Equilibrium (RCE) of two models exhibiting convective aggregation has been compared. The goal of the work, following the suggestion from the Radiative-Convective Equilibrium Model Intercomparison Project (RCEMIP), is to identify key parameters controlling self-aggregation in RCE for both models and discuss the processes controlled by these parameters in order to find the simulations similarities and to test their differences. The two models studied, the SAM (System for Atmospheric Modeling) and the ARPS (Advanced Regional Prediction System), have different physical and numerical formulations. This allowed us to compare the sensitivity to processes related to self-aggregation. When self-aggregation occurs, the two models present similar statistics for what concerns precipitation, warming, and drying of the atmosphere and anvil cloud area reduction (leading to an “Iris effect”), within the spread of the RCEMIP values. On the other hand, they differ both in the degree of organization and the organization feedback: SAM is strongly organized (is on the highest quartile of the RCEMIP for the Iorg Index) and the convective organization is achieved by cloud-radiative feedback; ARPS is weakly organized (on the multi-model average of the RCEMIP for the Iorg Index) and the moisture-convection feedback is leading to the convective organization. The prevalence of one mechanism over the other has been found in the interaction between the microphysics and the sub-cloud layer properties. This comparison suggests that, in order to have a robust measure of climate sensitivity, climate models should include both types of convective organization mechanisms as shown by the two models.

1 **Intercomparison of Convective-Aggregation States with** 2 **two Cloud Resolving Models**

3 **P. Bongioannini Cerlini¹, M. Saraceni², L. Silvestri²**

4 ¹University of Perugia, Centro Interuniversitario di Ricerca sull'Inquinamento e sull'Ambiente Mauro Felli
5 (CIRIAF) - Centro di Ricerca sul Clima e Cambiamenti Climatici (CRC), Perugia (PG)

6 ²University of Perugia, Department of Civil and Environmental Engineering (DICA) - Centro di Ricerca
7 sul Clima e Cambiamenti Climatici (CRC), Perugia (PG)

8 **Key Points:**

- 9 • The two models ARPS and SAM achieve a state of convective organization through
10 different mechanism and different degree of aggregation
- 11 • The predominance of clouds-radiative or moisture-memory feedback is dependent
12 on the initialization, microphysics and sub-cloud properties

Corresponding author: M.Saraceni, miriam.saraceni@studenti.unipg.it

Abstract

The Radiative-Convective Equilibrium (RCE) of two models exhibiting convective aggregation has been compared. The goal of the work, following the suggestion from the Radiative-Convective Equilibrium Model Intercomparison Project (RCEMIP), is to identify key parameters controlling self-aggregation in RCE for both models and discuss the processes controlled by these parameters in order to find the simulations similarities and to test their differences. The two models studied, the SAM (System for Atmospheric Modeling) and the ARPS (Advanced Regional Prediction System), have different physical and numerical formulations. This allowed us to compare the sensitivity to processes related to self-aggregation. When self-aggregation occurs, the two models present similar statistics for what concerns precipitation, warming, and drying of the atmosphere and anvil cloud area reduction (leading to an “Iris effect”), within the spread of the RCEMIP values. On the other hand, they differ both in the degree of organization and the organization feedback: SAM is strongly organized (is on the highest quartile of the RCEMIP for the Iorg Index) and the convective organization is achieved by cloud-radiative feedback; ARPS is weakly organized (on the multi-model average of the RCEMIP for the Iorg Index) and the moisture-convection feedback is leading to the convective organization. The prevalence of one mechanism over the other has been found in the interaction between the microphysics and the sub-cloud layer properties. This comparison suggests that, in order to have a robust measure of climate sensitivity, climate models should include both types of convective organization mechanisms as shown by the two models.

Plain Language Summary

The Radiative-Convective Equilibrium is a paradigm for atmospheric modeling of the tropics. In such a paradigm, the clustering of clouds can spontaneously occur and it can substantially affect the energy budget of the climate system. To study this phenomenon, we selected two models, with different numerics and physics, and we investigated the equilibrium statistics. We compared our results with the ones of the Radiative-Convective Equilibrium Model Intercomparison Project, where different models were used. We found similar precipitation, warming, and drying of the atmosphere, between the two models and that experiment. Instead, we found different types of cloud clusters and different feedback processes leading to this clustering. We attributed this difference to the representation of cloud formation processes in the two models and the initial properties of the layer below the clouds. This might have implications for the change in clouds with warming within the climate system.

1 Introduction

The radiative-convective equilibrium (RCE) of an ensemble of clouds has been used as a paradigm of a statistical equilibrium state of the atmosphere able to mimic the tropical part of the climate system. Given the crucial importance of moist convection inside the climate system and how to parameterize it inside climate models, RCE simulations have been used as a proxy to study the link between global circulation and convection (Held et al., 1993; Randall et al., 1994; Pauluis & Held, 2002b, 2002a). After these initial numerical studies, a number of additional studies were performed using RCE as a starting point to study the variability and organization of convection over a wide range of space and time scales. Among the different approaches used to evaluate convective variability, there was: the simulation of RCE states to study the predictability of rainfall at high resolution (Islam et al., 1993), the organization of convection (Robe & Emanuel, 1996), and the orographic variability of precipitation (Bongioannini Cerlini et al., 2005). Given the aims of these last simulations, different models were used with fixed imposed radiation and simplistic microphysical parametrization schemes, without ice phases of water content. The increased computing capability available made it possible to run three-

63 dimensional high-resolution simulations (Tompkins & Craig, 1998; Bretherton et al., 2005)
64 and to study the sensitivity of RCE states using models with enhanced dimensions of
65 the grid reaching the dimensions of mesoscale processes, with explicit moist variables and
66 different physics parameterizations.

67 The characteristic that arose further the attention over the RCE simulations was
68 the spontaneous development within these simulations of the convective organization (self-
69 aggregation) using cloud resolving models. Such models can simulate the space-time statis-
70 tics of an ensemble of clouds (Khairoutdinov & Randall, 2003) over domain sizes with
71 spatial extension up to hundreds of kilometers and for a length of time much longer than
72 that of a single cloud over homogeneous surface conditions. Despite the differences in
73 parametrizations packages (e.g. microphysics, radiation, turbulence) between models,
74 they showed in some cases spontaneous self-aggregation of clouds (Tompkins & Semie,
75 2017; Khairoutdinov & Emanuel, 2010; Jeevanjee & Romps, 2013; Ruppert Jr & Hoheneg-
76 ger, 2018; Holloway & Woolnough, 2016; Hohenegger & Stevens, 2016).

77 Generally, it has been pointed out that convective organization is the result of feed-
78 back between moisture-convection-radiation, which can be related to various processes
79 (C. Muller et al., 2022; Wing et al., 2017). Bretherton et al. (2005) and C. J. Muller and
80 Held (2012) found that a low level circulation from the dry to moist regions, forced by
81 longwave radiative cooling in the lower troposphere, is responsible for self-aggregation,
82 by transporting moist static energy (MSE) up-gradient. Wing and Emanuel (2014) us-
83 ing a MSE variance budget confirmed such a mechanism. On the other hand, C. Muller
84 and Bony (2015) found that aggregation could be obtained by suppressing rain evapo-
85 ration, even in the absence of radiative feedback. This mechanism was called “moisture-
86 memory aggregation”, where moist regions remain moist, thus more favorable to con-
87 vection (Tompkins, 2001b; Craig & Mack, 2013).

88 Given the differences among models, the need for comparison among them, with
89 different dynamical formulations, has been stated recently in different studies (Tompkins
90 & Semie, 2017; Wing et al., 2017, 2018). The impact of different model representations
91 of cloud physics and convective processes has been recognized as a key point to assess
92 the closeness between model self-aggregation to the atmospheric convective organization
93 and to compare the climate sensitivity to self-aggregation feedback as represented by mod-
94 els (Wing et al., 2020). How to assess the robustness of statistical variability and its close-
95 ness to the observed variability of tropical convection for simulations of RCE states (where
96 convective variables show self-aggregation), is one of the reasons for the work done within
97 the Radiative-Convective Equilibrium Model Intercomparison Project (RCEMIP) ex-
98 periment. In fact, within RCEMIP, the different models used, one-dimensional, three-
99 dimensional, and global, were driven to a radiative-convective equilibrium, using a pre-
100 defined protocol to start from conditions that were as similar as possible. Despite this,
101 since the equilibrium state is achieved in a statistical sense, and given the differences in
102 the convection simulations of the RCEMIP models spectrum, the different sensitivity to
103 various climatic parameters produced different results. Furthermore, it was underlined
104 that different model responses are linked to differences in models physics and numerics
105 (Wing et al., 2020). Thus, the question remains as to which factors in the models are
106 prevalent in aggregation.

107 For these reasons, this study sets out to compare two models in their reproduction
108 of convection statistics: The Advanced Regional Prediction System (ARPS, Oklahoma
109 University (OU), (Xue et al., 2000, 2001)) and the System of Atmospheric Modeling (SAM)
110 (Khairoutdinov & Randall, 2003). ARPS is a state-of-the-art reference model from its
111 use in three-dimensional simulations based on a non-hydrostatic formulation of conser-
112 vation equation for momentum, energy, and water variables used for Numerical Weather
113 Predictions (NWP) (Xue et al., 2014; Sun et al., 2021). It is recalled here that this model,
114 although very similar to the most common WRF model (Skamarock et al., 2005), was
115 not included in the RCEMIP (Wing et al., 2020). Therefore, this is the first study that
116 investigates self-aggregation with such a model.

117 The SAM model, based on an anelastic approximation, is formulated to conserve
 118 the liquid/ice static energy, which is a standard variable to study an ensemble of clouds
 119 that is continuously forced in a RCE simulation. Thus, SAM has been used extensively
 120 to study convective self-aggregation (Bretherton et al., 2005; Wing & Emanuel, 2014)
 121 and it is the model on which the aggregation theory was based (C. J. Muller & Held, 2012;
 122 Emanuel et al., 2014).

123 The objective of this paper is to see how an aggregated state of convection is achieved
 124 when ARPS is run in its standard setting and to compare it to the state achieved by the
 125 SAM model. The aggregation of convection is in fact an indication of the internal os-
 126 cillation of the model in an RCE configuration that is not used in the basic model setup.
 127 This configuration, where the boundary conditions are periodic and the lateral energy
 128 transport is absent, causes the model to reproduce a statistical oscillation within the sys-
 129 tem. By reaching the statistical equilibrium of precipitation, one can study the statis-
 130 tical oscillation of convection within the model, and its intrinsic process of convective
 131 organization, thus comparing the dominant processes in convection in the two families
 132 of models. We want to understand what kind of processes are dominant for this type of
 133 convection aggregation and to understand how similar or different these processes are
 134 when used on tropical/global scales.

135 Since the ways in which convection is organized depends on both the dimension-
 136 ality of the domain (C. J. Muller & Held, 2012; Patrizio & Randall, 2019) and the in-
 137 trinsic characteristics of the models (Wing et al., 2020; Yang & Tan, 2020; Pope et al.,
 138 2021), it is possible that the mode of internal equilibrium of the two models analyzed
 139 may contain information about the mode of oscillation of the climate system, that com-
 140 bines both oscillations of the compared models. This idea comes from the results of RCEMIP,
 141 where the degree of self-aggregation in SAM-CRM is outside the multi-model spread,
 142 while the WRF-CRM one is on the multi-model average. ARPS statistic, for the listed
 143 parameters that can be compared, appears to be average with many of the models used,
 144 and distant from the SAM statistic.

145 Thus, the research questions posed by this study are:

- 146 • What are the statistical properties of convection when each of the models reaches
 147 a stable state?
- 148 • Is the internal oscillations leading to similar aggregation processes (in terms of the
 149 statistical stability of convection) in the two models?

150 In Section 2 the two models, the numerical simulation setup and the initialization are
 151 described. In Sections 3 and 4 the results of the convective organization statistics, the
 152 cloud properties, and the convective organization feedback are described and discussed.
 153 In Section 5 a summary of the work is given.

154 2 Numerical Simulations

155 2.1 The SAM model

156 The first simulation is performed by using the System of Atmospheric Modeling
 157 (SAM version 6.10.6, Khairoutdinov & Randall, 2003). SAM solves the anelastic con-
 158 tinuity, momentum, and scalar conservation equations. The prognostic thermodynamic
 159 variables are the total non precipitating water ($q_T = q_v + q_c + q_i =$ water vapour +
 160 cloud water + cloud ice), the total precipitating water ($q_p = q_r + q_s + q_g =$ rain +
 161 snow + graupel) and the liquid/ice static energy, $h_L = c_p T + gz - L_v(q_c + q_r) - L_s(q_i +$
 162 $q_s + q_g)$, with L_v and L_s being the latent heat of vaporization and sublimation, respec-
 163 tively. By definition, h_L is conserved during the moist adiabatic processes (including freez-
 164 ing/melting of precipitation).

165 Given h_L , q_T and q_p , the mixing ratio of the various hydrometeors (q_c , q_i , q_r , q_s ,
 166 q_g) is diagnosed by partitioning relationships that depend only on temperature. The di-

167 agnosed mixing ratios are used to compute the water sedimentation and hydrometeor
 168 conversion rates through a bulk microphysics scheme, where the autoconversion of cloud
 169 water into rain is evaluated through the Kessler scheme, while ice aggregation is parametrized
 170 similarly to Lin et al. (1983). Cloud ice is considered as non-precipitating water but it
 171 is allowed to fall with its own terminal velocity $V_{TI} = 0.4$ m/s (Khairoutdinov & Ran-
 172 dall, 2003).

173 Longwave and shortwave radiative fluxes are computed using the radiation code
 174 from the National Center for Atmospheric Research (NCAR) Community Atmosphere
 175 Model (CAM version 3.0, Collins et al., 2006).

176 We choose a first-order Smagorinsky closure scheme for subgrid-scale (SGS) tur-
 177 bulence. The same SGS parametrization was used in previous studies by Bretherton et
 178 al. (2005); C. J. Muller and Held (2012); Wing and Emanuel (2014). Surface fluxes are
 179 interactively computed according to the Monin-Obukhov similarity theory.

180 2.2 The ARPS model

181 The second simulation is performed by using the Advanced Regional Prediction Sys-
 182 tem (ARPS version 5.3.4, Xue et al., 2000, 2001). ARPS solves the fully compressible
 183 conservation equations for mass, momentum, heat, and water substance (water vapor,
 184 liquid, and ice). The thermodynamic prognostic variables are the potential temperature,
 185 pressure, and the mixing ratio for six water species (water vapor, q_v , cloud water, q_c , cloud
 186 ice, q_i , rain, q_r , snow, q_s and hail, q_h).

187 Precipitation is computed through a bulk microphysics scheme where autoconver-
 188 sion of cloud water into rain is evaluated through the Kessler scheme (Kessler, 1969) and
 189 ice aggregation is treated with the three ice categories (cloud ice, snow, and hail or graup-
 190 pel) scheme of Lin et al. (1983).

191 The radiation code is adopted from the NASA/Goddard Space Flight Center, with
 192 shortwave radiative fluxes based on the model of Chou (1990) and longwave radiative
 193 fluxes based on the model of Chou and Suarez (1994). Surface fluxes are computed ac-
 194 cording to the Monin-Obukhov similarity theory and a first-order Smagorinsky scheme
 195 has been chosen for turbulence closure.

Table 1. Main properties of the two numerical models and simulations: the model version; the horizontal resolution, Δx ; the size of the squared domain; the initial sounding used to start the run (see Figure ??); the total running time; the radiation, microphysics, sub-grid scale mixing and surface fluxes parametrizations.

	SAM	ARPS
Model version	6.10.6	5.3.4
Δx (km)	3	3
Domain size (km)	768	1152
Initial sounding	SND-301 (Figure ??)	SND-296 (Figure ??)
Run time (days)	160	158
Radiation (Fully interactive)	CAM version 3.0 (Collins et al., 2006)	NASA/ Goddard (Chou, 1990; Chou & Suarez, 1994)
Microphysics	Original SAM single-moment (Khairoutdinov & Randall, 2003)	Warm-rain Kessler scheme (Kessler, 1969), Ice Lin scheme (Lin et al., 1983)
Subgrid-scale mixing	First-order Smagorinsky	First-order Smagorinsky
Surface fluxes (Fully interactive)	Monin Obukhov similarity	Monin Obukhov similarity

196

2.3 Numerical setup and initialization

197

198

199

200

201

202

203

204

205

206

207

The SAM simulation is performed over a doubly periodic domain with size $768 \times 768 \text{ km}^2$ and a uniform horizontal resolution of 3 km. We use 64 vertical grid levels with a rigid lid at the top at about 27 km. The first level is at 25 m and grid spacing gradually increases from 50 m near the surface to 500 m above 5 km. Then, it increases again from 500 m to 1 km above 20 km. Newtonian damping is applied to all prognostic variables in the upper third of the model domain (above 18 km). At the bottom, there is an oceanic surface with a constant sea surface temperature of 302 K, which is usually considered as the lower limit for self-aggregation to happen (Wing & Emanuel, 2014). The simulation is run with fully interactive radiation as done in Stephens et al. (2008); C. Muller and Bony (2015); Ruppert Jr and Hohenegger (2018). There is no mean wind and no rotation.

208

209

210

211

212

213

214

The ARPS simulation has a horizontal resolution of 3 km, with a large domain of 1152 km in length. We use 62 vertical levels with a rigid lid at the top at about 25 km. The first level is at 35 m and grid spacing is 35 m up to 140 m. Then the vertical grid is gradually stretched from about 70 m to about 700 meters up to 20 km. Above 20 km the grid spacing is about 800 m. Rayleigh damping is applied above 19 km. The simulation is run with fully interactive radiation, no mean wind, no rotation, and with an oceanic surface at a constant SST of about 302 K.

215

216

217

218

219

220

221

The main properties of numerical models and simulations are summarized in Table 1. Both simulations run for about 160 days. SAM runs with a time step of 10 s, while ARPS run with a time step of 6 s. Output fields are generated every 6 hours. The SAM simulation is initialized with a sounding obtained from a previous run of the SAM model in RCE equilibrium without self-aggregation (SND-301, see Supplementary Figure S1a). Convection is initiated by adding white noise to h_L in the lowest five levels, with an amplitude of 0.1 K in the lowest level linearly decreasing to 0.02 K in the fifth level.

222

223

224

225

226

227

228

ARPS is initialized with a colder and drier profile (SND-296, see Supplementary Figure S1b) which is obtained by running an 80-days simulation over a small domain (96 km x 96 km). This smaller simulation was initialized with the SND-301 profile. The new initialization profile, SND-296, is obtained by averaging mean temperature and water vapor on the smaller domain over the last 10 days, when statistical equilibrium is reached. Convective motions are initialized by applying a random perturbation of magnitude 0.2 K to the potential temperature field over the whole domain.

229

230

231

232

233

234

235

236

237

238

239

240

241

242

243

244

245

246

The initial colder and drier profile of ARPS turns out to be crucial for later stages of convective aggregation. Therefore we briefly introduce here some elements leading to the decrease in temperature and humidity of the ARPS domain. A more in-depth discussion will be provided in Section 4. Figure 1a shows the non-aggregated state of the small domain simulation after 75 days. Precipitable water (Figure 1b) drops very quickly from about 60 mm to 42 mm, while the daily precipitation rate exhibits an opposite behavior by increasing abruptly to about 6.5 mm/day (Figure 1b). After a few days of simulation, the small domain is entirely covered by a very thin anvil cloud which remains there until the end of the simulation (Figure 1c). The average cooling and drying of the ARPS domain are due to the presence of such an anvil which blocks the incoming solar radiation. Such high cloud fraction over small domain simulations of RCE has been found also during the RCEMIP project by Wing et al. (2020) (see Figure 9 in the article) and therefore it is not related only to the specific model configuration. When initializing the large domain ARPS simulation (following the RCEMIP protocol by (Wing et al., 2018)), the cloud water and ice at 12 km, produced by the smaller domain, are removed (Figure 1c), removing the large anvil, while leaving its effect on the vertical profile of temperature and water vapor. Therefore convective motions of ARPS start in a drier and colder domain than those in SAM.

247

248

249

The main mechanisms behind the anvil formation in the ARPS small domain rely on the properties of the microphysics scheme adopted by the model, as mentioned in the previous section. Further details are provided in Section 4.

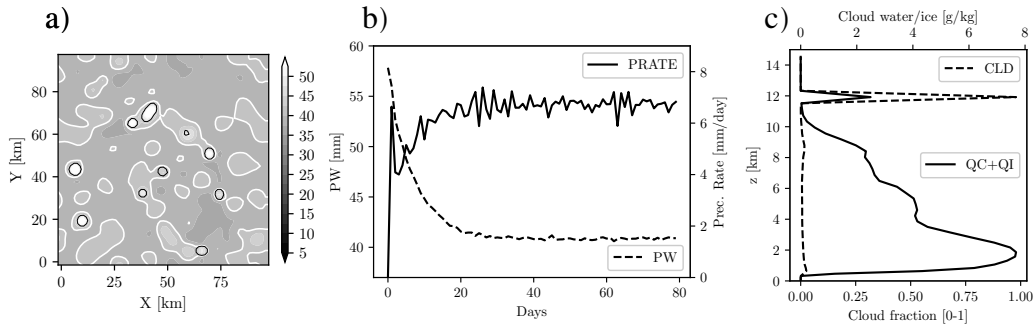


Figure 1. Snapshots of PW at day 75 (midnight) on the small domain used to initialize ARPS simulation (same contours and colors used in Figure 2) (a). Time evolution of daily averaged precipitation rate and precipitable water over the ARPS small domain (b). Cloud fraction and total cloud condensate averaged over the last 20 days of the small domain simulations (c).

3 Results

3.1 Statistics of convective organization

In SAM and ARPS simulations The precipitation rate reaches a statistical equilibrium, with similar values of 4.2 mm day^{-1} in SAM and of 4.1 mm day^{-1} in ARPS. The domain average statistics of the simulations final stages are reported in Table 2. In SAM, a RCE state is reached, where the Total Heat flux (THF, sum of the latent heat flux LHF and sensible heat flux SHF) is in balance with net column radiative cooling (R_{NET}), and the LHF, which dominates the THF, is in balance with precipitation (Precip) (see Table 2). In ARPS, instead, the net atmospheric energy imbalance, F_{NET} , is greater than in SAM ($F_{NET} = 4.16 \text{ W m}^{-2}$), reaching a value similar to that obtained for the model WRF in RCEMIP (see Table 2).

Both model simulations present the convective organization as it is shown by the Precipitable Water (PW) pattern evolution in Figure 2. The convective organization is marked by the clustering of convection, as underlined in Figures 2d and 2h for ARPS and SAM respectively, when precipitation equilibrium is reached. There is a marked intensely convecting moist patch surrounded by a region of dry subsiding air (Bretherton et al., 2005).

By looking at the evolution of the two simulations, it can be noted that in SAM the convective organization is achieved with the expansion of dry regions, with suppressed precipitation, that seclude a moist region where convection occurs. In ARPS, such expansion is not as evident as in SAM.

In SAM, the PW pattern is uniform until the 40th day, when a dry patch at $x = 400 \text{ km}$ starts to form (see Figure 2f and the *Homvöeller* diagram of the PW in supplementary Figure S2a). Between days 40-80, the system evolves into an organized state, with the dry patch covering most of the domain at the equilibrium (after day 100). In ARPS, instead, the PW pattern is uniform until day 20 when some moist patches and two dry patches form at $x = 400 \text{ km}$ and $x = 800 \text{ km}$ (see Figure 2b and the *Homvöeller* diagram of the PW in supplementary Figure S2b). By day 60 the moist regions converge into a single moist patch when the equilibrium state is reached, with a moist region surrounded by a drier region (see also Supplementary Figure S2b).

There is a difference between the dimensions of the developing convective clusters. Regarding SAM, the dry zones are very large compared to the moist zone, where convection is taking place, covering almost the 90% of the whole domain (Figure 2h). The convective cluster in SAM has a diameter of nearly 300 km. For ARPS instead, the or-

Table 2. RCE average statistics over the aggregated state (days 135-140) of simulations, following Table A2 of Wing et al. (2020). The values for the RCEMIP SAM-CRM model, RCEMIP WRF-CRM model, and the average (\pm the standard deviation) of RCEMIP models are reported in the last three columns for a direct comparison. Such values are directly taken from Table A2 or the text of Wing et al. (2020). \mathbf{F}_{NET} is the atmospheric energy imbalance, that is the magnitude of the difference between R_{NET} and the total surface thermal fluxes; R_{NET} is the column integrated atmospheric radiative forcing (negative values indicates net atmospheric radiative cooling) which is obtained directly by column integration of the radiative forcing (quad, prognostic variable); LHF and SHF are surface latent and sensible heat (positive values indicates fluxes into the atmosphere); PW is the precipitable water; Precip. is the daily precipitation rate; LWP and IWP are the cloud liquid water path and cloud ice water path respectively. LR is the tropospheric (15 km) Lapse Rate; T_s , RH_s are respectively the absolute temperature and the relative humidity at the lowest model level.

Var	Unit	SAM	ARPS	RCEMIP-SAM	RCEMIP-WRF	RCEMIP-AVG (STD)
\mathbf{F}_{NET}	W m^{-2}	4.16	26.15	3.87	21.73	4.12 (± 5.66)
R_{NET}	W m^{-2}	-122.80	-102.46	-118.05	-106.54	-110.17 (± 16.08)
LHF	W m^{-2}	120.26	65.46	113.15	90.37	101.93 (± 15.29)
SHF	W m^{-2}	6.71	10.85	8.77	37.90	11.16 (± 5.74)
PW	mm	25.7	38.1	31.2	41.2	32.8 (± 4.1)
Precip.	mm day^{-1}	4.2	4.1	3.9	3.1	3.5 (± 0.5)
LWP	mm	0.056	0.015	0.048	0.065	0.041 (± 0.028)
IWP	mm	0.015	0.001	0.025	0.097	0.037 (± 0.038)
LR	K km^{-1}	-6.68	-7.08	-7.2	-6.91	-6.83 (± 0.65)
T_s	K	300.3	298.4	n/a	n/a	n/a
RH_s	%	64	75	n/a	n/a	73 (n/a)
lorg		0.9	0.6	0.9	0.5	0.6 (n/a)

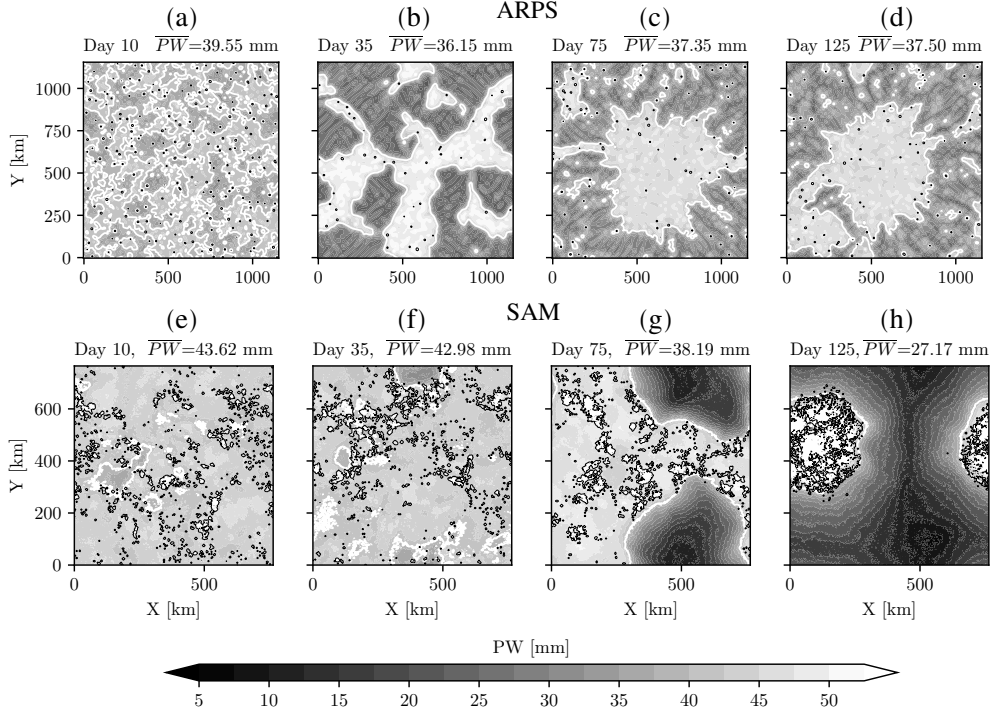


Figure 2. Time evolution of Precipitable Water (PW, filled contours) for ARPS (a,b,c,d) and SAM (e,f,g,h) simulations. The region where aggregation occurs is moister and presents a higher PW (lighter colors). For both models snapshots are taken on midnight after 10 (a,e), 35 (b,f), 75 (c,g) and 125 (d,h) days. The thick white line represents the boundary between moist and dry patches, taken as $PW=40$ mm. Black lines are contours of total water condensate of 0.4 g/kg at a height of 1.5 km, representing low-level clouds. It is important to recall here the different scales on the X and Y-axis.

284 ganization of convection comes with dry areas that cover near the same percentage of
 285 the moist areas, with 40% of the simulation domain covered by the convective cluster,
 286 which has a diameter of approximately 550 km (Figure 2d). The greater domain size of
 287 ARPS could have influenced this percentage, by allowing the formation of multiple clusters
 288 (as is evident in Figure 2d), as it has been found in previous studies (Stephens et
 289 al., 2008; Wing et al., 2018; Patrizio & Randall, 2019).

290 The difference underlined by PW patterns can be further explained by looking at
 291 the moisture sorted time series of the Water Vapor Path (WVP) (Figure 3). These are
 292 computed by dividing the two simulations domain into blocks of equal area (96 km²),
 293 and then sorting them into four quartiles from driest to moistest, based on their daily
 294 WVP.

295 Figure 3a shows that while in SAM there is a very large inter-quartile difference,
 296 especially between the driest and moistest quartiles, in ARPS this difference is smaller.
 297 Indeed, for SAM, as in (Bretherton et al., 2005), the driest WVP quartile is the one that
 298 decreases most dramatically from day 25 until day 75 by about 27 g/m², when the or-
 299 ganization is developing, while the moistest quartile increases in WVP of about 3 g/m².
 300 Instead in ARPS, the moistest and driest quartiles seem to be 5 g/m² higher and 5 g/m²
 301 lower than the WVP domain daily mean respectively, after organization occurs (Figure
 302 3b).

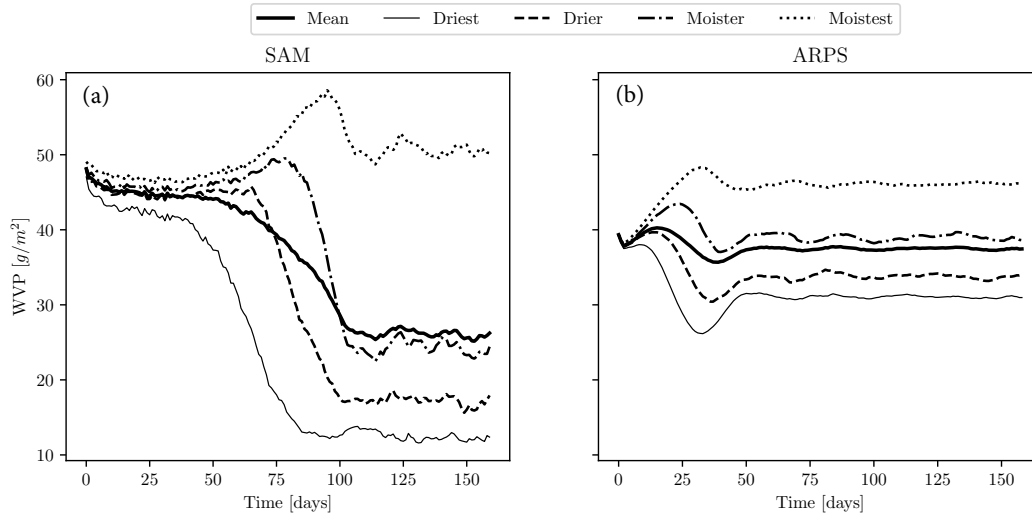


Figure 3. Moisture-sorted time series of the daily averaged Water Vapor Path (WVP) g/m^2 for SAM (a) and for ARPS (b). The thick lines are the domain mean and the other curves are the means over the $96 km^2$ blocks sorted into four quartiles based on their daily WVP.

303 In both SAM and ARPS, WVP increases only in the quartiles where deep convec-
 304 tion is taking place and decreases in the dry regions. This is also reflected by the pre-
 305 cipitation quartiles (not shown), in which after aggregation has occurred, the moister and
 306 moistest quartiles present precipitation, while in the driest and drier quartiles, it is ab-
 307 sent. However, the equilibrium is reached in both models, where the whole system reaches
 308 its statistical equilibrium, and the PW oscillates around a mean value (Figure 4d).

309 Convective organization in both SAM and ARPS has the same impact on the sim-
 310 ulated atmosphere, leading to its warming and drying, as it is reported in Figure 4a 4b
 311 and 4c. The warming produced by the organization process can be inferred from the mean
 312 state profiles of MSE, Temperature (T), and Relative humidity (RH) averaged at equi-
 313 librium (between 135-140 days) over the whole domain with respect to the initial ones
 314 (averaged between the first 5-10 days).

315 In fact, in the case of SAM, we notice a decrease of MSE in the lower troposphere
 316 (around 2 km), due to the general drying of the atmosphere, and growth of MSE in the
 317 upper troposphere due to warming (Figure 4a). In ARPS, on the other hand, it can be
 318 seen that the MSE profile is initially dryer than the SAM one and remains dry in the
 319 lower troposphere, while it warms up at equilibrium with an MSE growth occurring in
 320 the mid-troposphere. The warming is underlined by the increase in temperature (Fig-
 321 ure 4b) in both simulations, while the drying can be noted in Figure 4c with the rela-
 322 tive humidity decreasing in the whole troposphere in both simulations, and in Figure 4d
 323 where the PW is shown to decrease with the organization in both SAM and ARPS.

324 These results are in line with the main results of the RCEMIP (Wing et al., 2020)
 325 who found that there is a robustness of the results on heating and drying of the mean
 326 state with convective organization among models. The temperature and relative humid-
 327 ity profiles of both SAM and ARPS are within the ensemble spread of RCEMIP mean
 328 state profiles (see Figures 7 and 8 of (Wing et al., 2020)). However, SAM final state is
 329 warmer and drier than the ARPS one (Figure 4). This is also evident from the values
 330 at the surface shown in Table 2, which are near the RCEMIP range values. The surface
 331 relative humidity (RH_s) is 64% for SAM and 75% for ARPS and the surface temper-
 332 ature (T_s) is 300.3 K for SAM and 298.4 K for ARPS. As already stated in the previ-

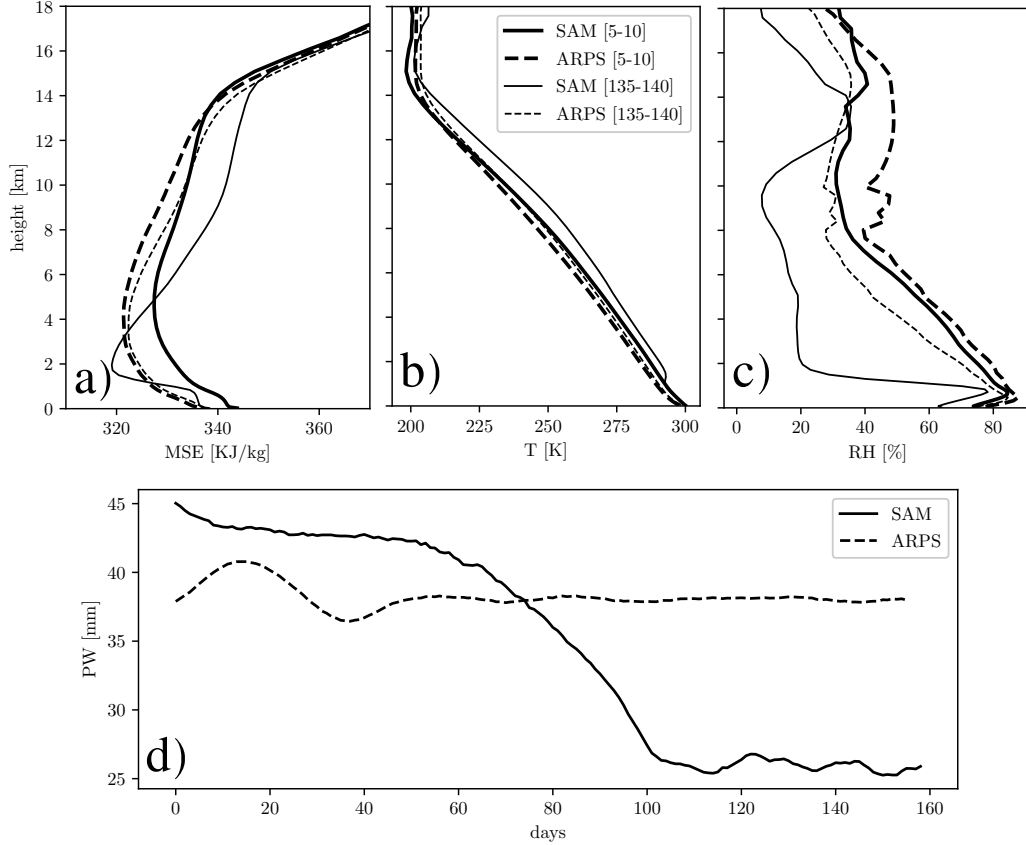


Figure 4. Horizontally averaged profiles of Moist Static Energy (MSE) (a), absolute Temperature (T) (b), and Relative Humidity (RH) (c) for the two simulations, averaged at the initial stage (5-10 days) and at the final aggregated state (135-140 days). Time evolution of Precipitable Water (PW) for both simulations (d). Precipitable water is evaluated by considering all condensates.

ous section, given the different initialization, ARPS starts already with an initial colder profile compared to SAM.

The warmer and drier final state of SAM is reflected also in the values of the surface fluxes (see Table 2). Given the smaller RH_s in the SAM model, the LHF_s are larger ($LHF = 120 \text{ W m}^{-2}$) than those of ARPS ($LHF = 65 \text{ W m}^{-2}$). On the other hand, given the smaller T_s of ARPS, the SHF_s are larger ($SHF = 11 \text{ W m}^{-2}$) than those of SAM ($LHF = 7 \text{ W m}^{-2}$). The same behavior is observed by comparison with the RCEMIP results from WRF and SAM models (see Table 2).

Regarding the state of the convective organization degree in the two models, we have decided to compute the Organisation index (Iorg) (Tompkins & Semie, 2017), which is shown in Figure 5a. It is a measure of the convective organization, which compares the nearest neighbor distribution of convective cores of the simulated and random convection. In ARPS it reaches an averaged daily value of 0.6 at equilibrium, a value much lower than the one of 0.9 attained by SAM at equilibrium. This is in agreement with the results of the RCEMIP project (Wing et al., 2020), where similar values were found for both models (see their Figure 12). The Iorg value reached by ARPS is closer to the average value of the multi-model comparison in RCEMIP (mean value of 0.6, see Table 2), while SAM is in the highest quartile among the models. Based on such metrics, we can

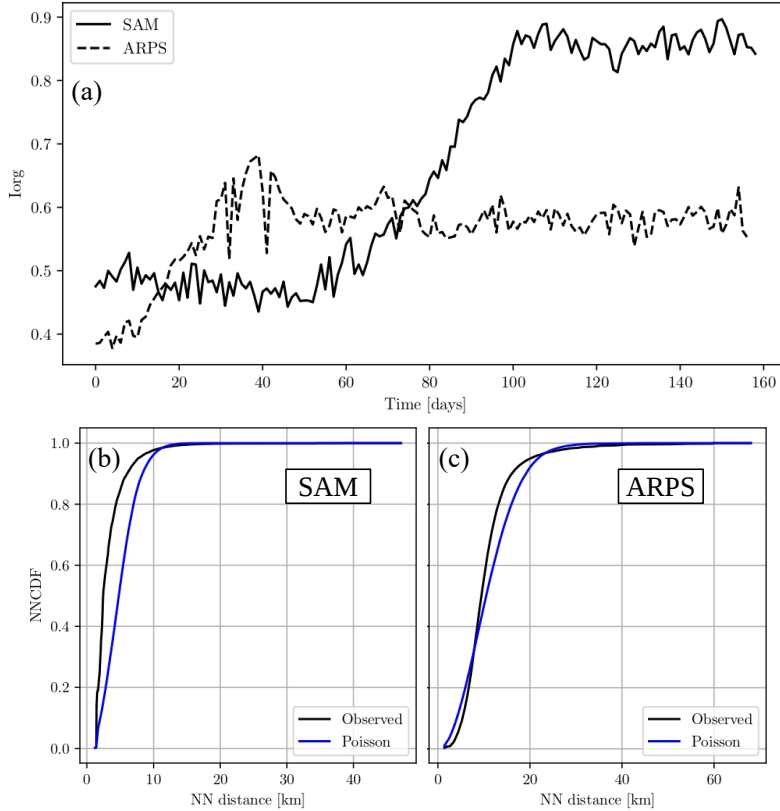


Figure 5. The daily Organization index (I_{org}) for SAM and ARPS, as computed by (Tompkins & Semie, 2017) is reported in (a), while the corresponding cumulative density function of the calculated Nearest Neighbor distances (NNPDF) versus nearest neighbor distance of observed and idealized Poisson convective distribution is displayed for SAM in (b) and for ARPS in (c).

351 infer that SAM undergoes a strongly organized convection, while in ARPS the organ-
 352 ization is weaker (Figure 5a).

353 The I_{org} evolution mirrors the evolution of the PW (Figure 4d) and that of the WVP
 354 (Figure 3). Interestingly, between days 35-40 in ARPS, the I_{org} index oscillates, reach-
 355 ing its maximum value of 0.7. This corresponds to a decrease in PW, caused by an ex-
 356 pansion of dry patches and a corresponding clustering of moist regions (see Supplemen-
 357 tary Figure S2b).

358 The observed cumulative density function of the calculated Nearest Neighbor dis-
 359 tances (NNPDF) in ARPS (Figure 5c) indicates the presence of regular convection at
 360 distances less than 10 km, while the clustering occurs at larger spatial scales, up to 60
 361 km. This regular convection is noticeable also in Figure 2c and Figure 2d, where shal-
 362 low clouds are regularly distributed over the domain. A similar distribution was obtained
 363 from WRF-RCE simulations (Tompkins & Semie, 2017) and also from satellites obser-
 364 vations of tropical convection (Semie & Bony, 2020). This regular convection is absent
 365 in SAM (Figure 5b), where the clustering of convection occurs immediately at very small
 366 spatial scales. Indeed, in Figure 2h only one cluster is present, made by very small and
 367 packed convective structures.

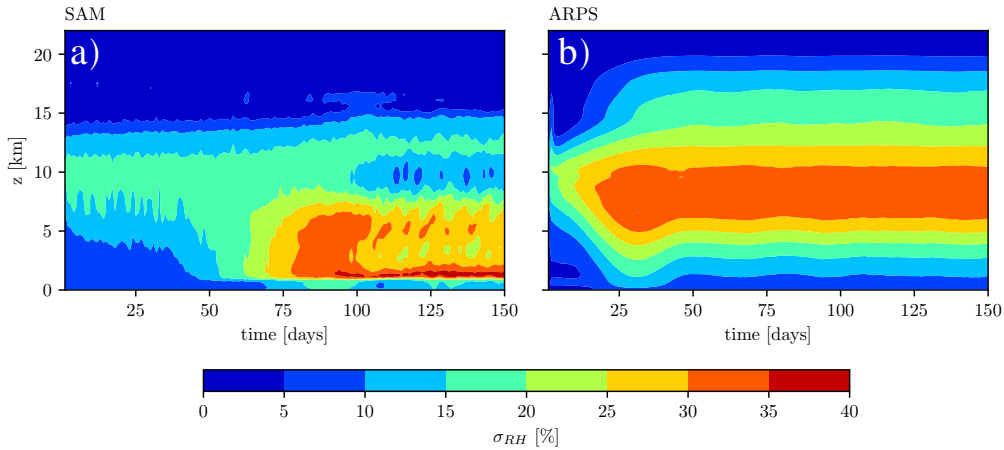


Figure 6. Temporal evolution of the domain averaged standard deviation of relative humidity (σ_{RH}) for the SAM (a) and ARPS (b) simulation.

368

3.2 Cloud properties

369

370

371

372

373

374

375

376

377

378

379

380

381

382

383

384

385

386

387

388

389

390

391

392

393

394

395

396

397

398

399

400

The evolution of the convection variability can be followed by looking at the domain averaged standard deviation of the relative humidity (σ_{RH}), as shown in Figure 6. After the initial time steps, there is a relevant perturbation at 10 km that amplifies in both models. Convection is occurring immediately after the initialization, starting from the middle troposphere, thus slightly increasing the σ_{RH} there. Then, for SAM (Figure 6a), after 75 days, the σ_{RH} starts increasing – reaching a value of around $\sigma_{RH} = 40\%$ – in the lower to middle troposphere (from 1.5 km to 7.5 km), as deep convection organizes. Instead, for ARPS, the initial perturbation starts expanding to all troposphere after 10 days, and then, after 25 days, the increase of σ_{RH} reaches its maximum in the middle troposphere, at 7.5 km with a value of $\sigma_{RH} = 35\%$, as convection organizes. Similar results to ARPS have been found in (Tompkins & Semie, 2017) for the WRF model.

From this analysis, it can be inferred that, although the convective organization is occurring in the two models, the type of convection is different. If in SAM the σ_{RH} increases especially in the lower troposphere, in ARPS this happens in the mid-troposphere, thus convection is located at different heights in the two models.

The difference in the cloud properties in the two models is underlined in Figures 7a, 7b, 7c and 7d, which show respectively the radiative forcing, the cloud fraction, the cloud water and the cloud ice at the initial stage (averaged between 5-10 days) of the considered simulations. As adopted in RCEMIP (Wing et al., 2020), a cloud is defined according to a threshold value of cloud condensate ($10^{-5} \text{ kg kg}^{-1}$ or 1% of the saturation mixing ratio over water, whichever is smaller).

The cloud fraction profiles at the initial state are very different among the two simulations, especially regarding the high-level clouds ($> 8 \text{ km}$). This is also visible in Figure S3, where anvil clouds evolution is shown. The peak high cloud fraction (“anvil”) is very large for ARPS: the ARPS anvil is located at 12 km and reaches an average value of cloud fraction of 0.9, and the cloud fraction is equally distributed between 10 and 15 km. On the other hand, SAM simulation develops an anvil with a much smaller average cloud fraction of 0.13 at 12 km height. (Khairoutdinov et al., 2022) showed that the single moment microphysics of SAM, as used in this article, underestimates the amount of high cloud. This is also visible from our results, where the high cloud fraction is much less than in the ARPS model, where different microphysics is used. The major difference in the microphysics parameterization between the two models is the presence of ice

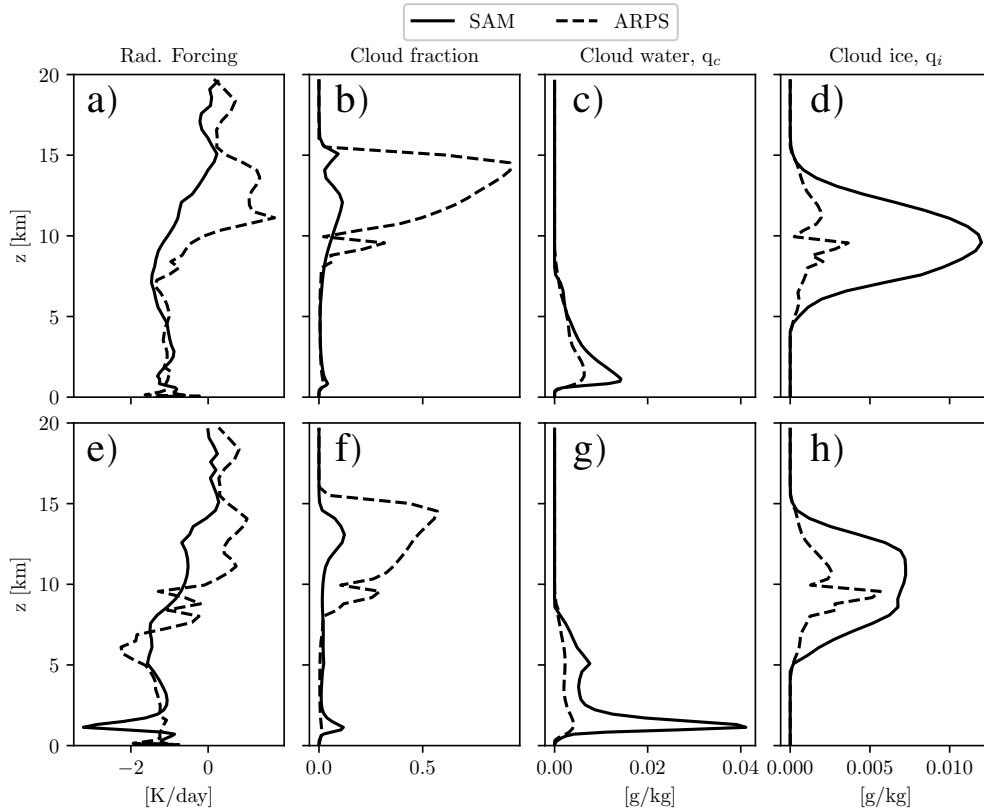


Figure 7. Radiative forcing, cloud fraction, cloud water, and cloud ice for the initial state (a,b,c,d) and the final state (e,f,g,h) of the two simulations. The initial (final) state is averaged over the days 5-10 (135-140) days for both simulations.

401 sedimentation, which in SAM is permitted, with an ice terminal velocity of 0.4 m/s . In
 402 Khairoutdinov and Randall (2003) it was verified that the presence of ice sedimentation
 403 in SAM leads to a reduced anvil below 9km. Thus, in the absence of ice sedimentation,
 404 the anvil in SAM would have been more extensive.

405 The thick anvil of ARPS heats the upper troposphere, while it cools the middle and
 406 lower troposphere (Figure 7a). In SAM there is cooling in all troposphere except for the
 407 top of the anvil at 15 km. This is because ice cirrus clouds act to reflect incoming short-
 408 wave radiation and entrap long-wave radiation from the clouds below (Liou, 1986; Schlimme
 409 et al., 2005). In both models, especially in ARPS, the effect of anvil clouds on the ra-
 410 diative heating profile is to warm near the cloud base and cool near the cloud top, as pointed
 411 out by (Hartmann & Berry, 2017).

412 With the convective organization, the anvil cloud fraction is greatly reduced both
 413 in ARPS and SAM as is shown in Figure 7f, while the low cloud fraction notably increases
 414 only in SAM. The presence of low clouds in SAM has been considered a necessary fac-
 415 tor for convective organization (C. J. Muller & Held, 2012; Wing & Emanuel, 2014; C. Muller
 416 & Bony, 2015), which increases with increasing resolution (Khairoutdinov et al., 2009).
 417 In general, the presence of low clouds in RCEMIP models is highly variable and presents
 418 a strong spread among CRMs in the mean state. The presence of low clouds in SAM com-
 419 pared to ARPS may be related to the formation of downdraft and in general to the tem-
 420 perature profile reached by the two models, as will be discussed in more detail in the fol-
 421 lowing sections.

Indeed, at the top of the boundary layer, SAM presents a simulated cloud fraction slightly higher than ARPS, with a cloud cover fraction > 0.1 and a higher content of q_c ($q_c = 0.015$ g/kg for SAM and $q_c = 0.009$ g/kg for ARPS). Then, the cloud water increases drastically in SAM with aggregation, with an equilibrium value of 0.04 g/kg, while in ARPS is slightly reduced (Figure 7g). The cloud ice decreases in SAM, almost by half, while increases in ARPS, reaching a value of 0.005 g/kg (Figure 7h). This is probably related to the ice to snow different conversion threshold used in the models microphysics scheme, being higher for ARPS than for SAM.

The correspondent radiative forcing in SAM is a pronounced cooling at 2 km of almost -4 K/day (see also the radiative forcing quartiles in Supplementary Figure S4). This marked cooling is absent in ARPS simulation because low clouds are too few and the cloud water is low. Around 6 km height, ARPS show a larger radiative cooling than that of SAM (Figure 7e). Such cooling comes mainly from the dry regions (see Supplementary Figure S4). One possible reason behind the difference between the SAM and the ARPS mid-tropospheric cooling is to be found on the different anvil properties. Ticker anvils are more efficient in blocking the removal of heat in the convective region, with respect to dry regions. Thus, a larger amount of heat must be transported to the dry regions and radiated out to space (Wing et al., 2017; Yang & Tan, 2020).

The spatial difference in cloud fraction between the two models is also shown in Figure 2, where the black dots represent the low clouds. In SAM the presence of low clouds is significant from the beginning of the simulation and increases with the organization of convection (Figure 2e and Figure 2h), while in ARPS the low clouds decrease with aggregation (Figure 2a and Figure 2d).

3.3 Convective organization feedback

The convective organized state in SAM is characterized by the onset of a virtual circulation of MSE from the dry to the moist regions (C. J. Muller & Held, 2012). The mesoscale circulation that develops with the organization can be visualized using the stream function Ψ (Bretherton et al., 2005), derived as the horizontal integral over vertical velocity starting from the driest column to the moistest, after having sorted them from lowest to highest Column Relative Humidity (CRH). The same sorting described in the previous section 3.1 is applied here, but in this case, it is done based on the CRH. By looking at the advective tendencies of MSE, implied by the stream function, one can capture the general mechanism of energy exchange between the columns. In SAM, the MSE “circulation” is imposed between the moist and dry columns only after the 50th day (not shown). By day 100, SAM has attained a state of convective organization. An up-gradient transport of MSE is visible (Figure 8a), with the low MSE being accumulated in the dry columns. In the moistest blocks (40-64) there is an inflow in the lowest level (1-2 km), while the outflow is mainly between 8 to 10 km. These fluxes are in correspondence with the presence of a deck of low clouds (Figure 8a).

This is in accordance with what is underlined in the equilibrium state sorted mass flux (taken as $M = \rho w$ with units of $kg\ m^{-2}s^{-1}$). Indeed in SAM, there is a pronounced updraft in the moist region at 1.5 km with the downdraft occurring in the moister and drier column (Figure 9c). Once convective aggregation has been imposed in the simulation, the sorted quartiles become divergent, compared to the initial days (Figure 9a).

In the dry quartiles there is a strong radiative cooling at the top of the moist boundary layer generated by low-level clouds, which drives subsidence (see Figure 7e and Supplementary Figure S4). The simulation shows pronounced cooling only at the top of the low clouds, formed in the moist columns. As C. J. Muller and Held (2012) has highlighted, this cooling generates subsidence in the dry regions, and the mid-level warming enhances the upward motion in the moist regions. The former induces a horizontal convergence of air from the moist columns to the subsidence top area, the latter instead corresponds to an upward flux raised by surface heat fluxes. To close the circulations a lateral inflow of dry air develops from dry columns to moist columns at low elevation (1 to 1.5 km).

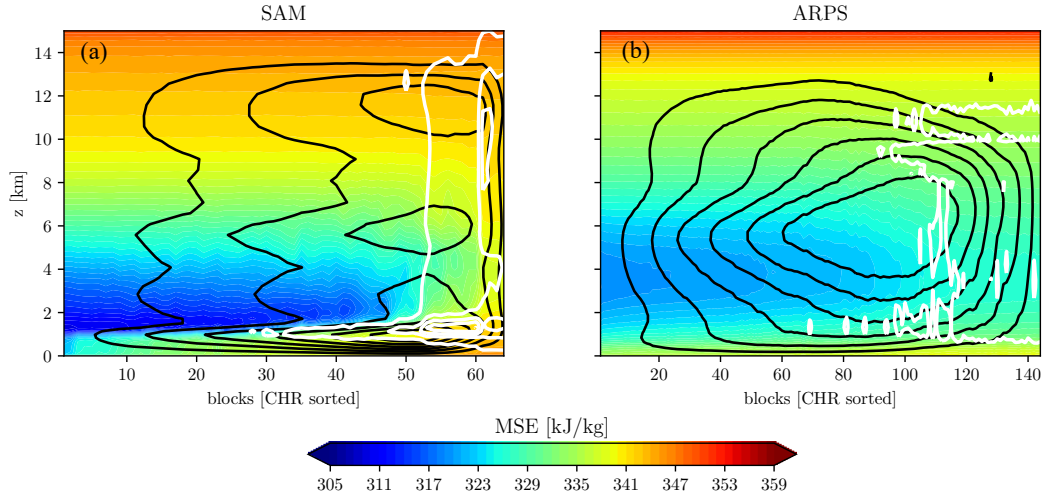


Figure 8. The average value of the MSE “circulation” between 135-140 days for SAM (a) and ARPS (b), with columns ranked by Column Relative Humidity (CRH), from driest to moistest. Black contours show the stream function Ψ (contour interval $0.05 \text{ kg m}^{-2} \text{ s}^{-1}$, starting at $0.01 \text{ kg m}^{-2} \text{ s}^{-1}$, solid for positive values and dashed for negative values) as a function of CRH and height. White contours show cloud condensate (cloud ice and cloud water) $q_N = q_i + q_c$ (contour interval 0.005 g/kg , starting at 0.001 mg/kg). Shaded contours represent MSE.

475 This circulation advectively diverges MSE out of the driest columns, increasing the MSE
 476 gradient.

477 This low-level cooling is purely attributable to longwave cooling produced by the
 478 presence of low clouds, as previously recognized in the literature (C. J. Muller & Held,
 479 2012; Wing & Emanuel, 2014; C. Muller & Bony, 2015). The low clouds, as stated also
 480 in the previous sections, are of primary importance for the onset of aggregation. By look-
 481 ing at Figure 8a one can see that they reach more than half of the sorted blocks, while
 482 the SAM anvil at equilibrium occupies only the moistest ones.

483 Emanuel et al. (2014) demonstrated similar feedback in a two-layer model where
 484 the phenomenon of self-aggregation is regarded as the result of the linear instability of
 485 the RCE state, which leads to deep convection and upward motion in part of the domain
 486 and dry air with few clouds in the rest, reconciling the stable equilibria of Sobel et al.
 487 (2007). The instability happens when a negative moisture perturbation leads the dry columns
 488 to become dryer, owing to an increased longwave cooling and the consequent downward
 489 motion. In the moist columns, a positive moisture perturbation leads them to enhance
 490 their upward motion by decreasing the long-wave cooling.

491 In ARPS, on the other hand, the “circulation” of MSE is not noticeable, both in
 492 the days before the organization (not shown) or once the simulation has reached the or-
 493 ganized equilibrium (Figure 8b). There is no sign of circulation below 2 km (as also no-
 494 ticeable in Figure 9d). Instead, there are updrafts in the moist regions, reaching their
 495 maximum at around 8 km, and downdrafts in the dry regions (see Figure 8b). This, rather
 496 than being a sign of the up-gradient transport of MSE, is a result of the occurrence of
 497 ARPS convective towers in the moist regions with downdrafts at the edges of these re-
 498 gions and in the remaining part of the dry domain. Also in Figure 8b, it can be seen the
 499 absence of low clouds covering the domain (as already pointed out in previous sections),
 500 as well as the greater size of the ARPS anvil compared to that of SAM.

501 The fact that the low-level circulation never appears in ARPS is also demonstrated
 502 by looking at the bottom layer wind speed at the boundary between the moist and the

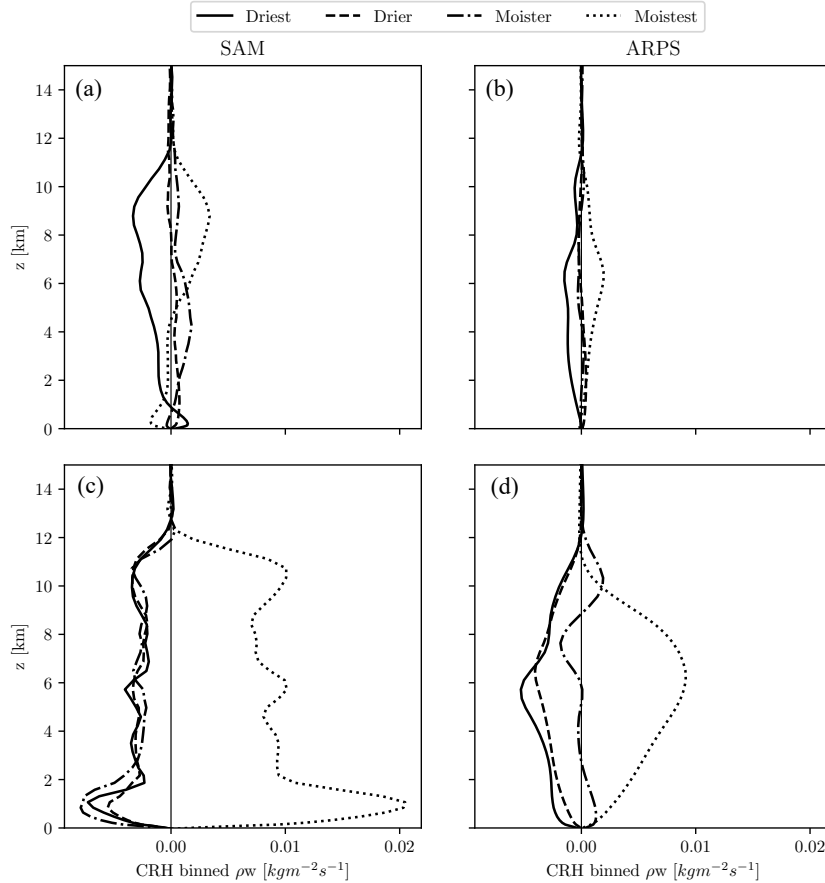


Figure 9. Average values of the CRH blocks-quartiles binned of the mass-weighted vertical velocity between the 5th and the 10th day for SAM (a) and ARPS (b), and between the 135th and the 140th day for SAM (c) and ARPS (d).

503 dry regions (see Figure 10c). While in SAM such velocity increases (which is a clear sig-
 504 nal of a radiatively driven aggregation as shown by Windmiller and Craig (2019), see their
 505 Figure 8), in ARPS it remains almost constant. Thus, rather than being a convective
 506 organization led by radiative feedback, there must be other processes at play in the ARPS
 507 model.

508 Indeed, C. Muller and Bony (2015) found another type of aggregation called “moisture-
 509 memory aggregation”, which is favored by weak downdrafts below clouds. Weak down-
 510 drafts can occur when the sub-cloud layer is nearly saturated and rain cannot evaporate.
 511 Figures 10a and 10b show that ARPS has a saturated sub-cloud layer both at the start
 512 (not shown) and at the end (Figure 10a) of the simulation. Instead, SAM never reaches
 513 such condition (Figure 10b). The saturation of the sub-cloud layer in ARPS directly in-
 514 fluences the downdrafts properties: ARPS downdrafts are weaker than those in SAM and
 515 they cover a smaller fraction of the domain (see Supplementary Figure S5). This again
 516 does not favor the radiative aggregation which is mostly sustained by downdrafts induced
 517 by the radiative cooling above shallow clouds.

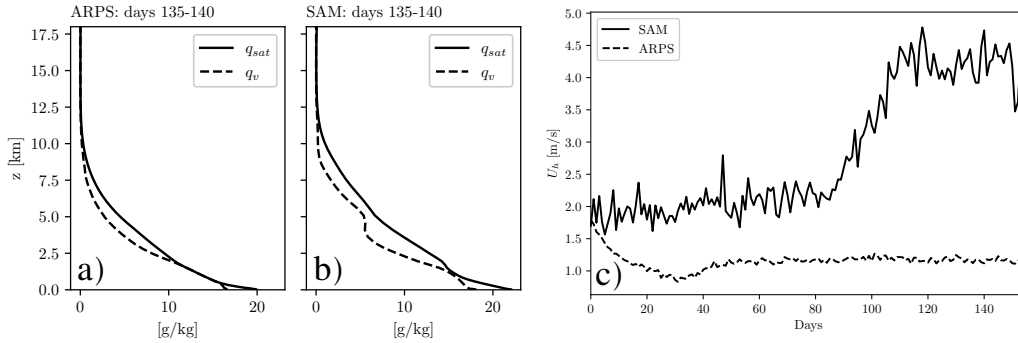


Figure 10. Vertical profiles of ARPS saturation water vapor mixing ratio (q_{sat}) and water vapor mixing ratio (q_v) over cloudy grid points (defined as grid points at 1.5 km height where the total cloud water condensate exceeded 10^{-3} g/kg) between days 135 and 140 a); b) same as a) but for SAM simulation; time evolution of bottom layer horizontal wind speed (U_h) averaged over the boundary between moist and dry patch (identified with the same criterion as in Figure 2) c).

518

4 Discussion

519

In the literature, (C. Muller & Bony, 2015; C. J. Muller & Held, 2012; Wing & Emanuel, 2014; Tompkins & Semie, 2017; Coppin & Bony, 2015) many experiments have been carried out in order to assess the sensitivity of convective organization to different choices of physical parameters and processes within the same CRM. Here we wanted to study the same robustness of the convective organization process found within the same model, by using two different models. In particular, we recognize different physical mechanisms leading to the convective organization in the ARPS and SAM model.

526

In general, the SAM model undergoes a "radiative aggregation" (Emanuel et al., 2014), where the MSE up-gradient circulation, driven by the contrasting radiative cooling rates between the moist and the dry regions, is the main driver of convective aggregation (C. J. Muller & Held, 2012). On the other hand, the organized state in the ARPS model does not exhibit such MSE circulation (Figure 8), but it can be traced back to a "moisture-memory aggregation" (C. Muller & Bony, 2015; C. Muller et al., 2022) or moisture-convection feedback (Tompkins, 2001b).

533

534

535

536

537

538

539

540

541

542

543

544

545

546

547

548

549

C. Muller and Bony (2015) found a similar result within the SAM model, by weakening the effect of cold pools. In particular, the moisture memory aggregation was favored by weaker downdrafts below clouds, which can occur when the sub-cloud layer is nearly saturated and rain cannot evaporate. Such condition has been verified in ARPS by looking at the profiles of the water vapor saturation mixing ratio (Figure 10), where the sub-cloud layer is saturated between 1 and 2.5 km both at the start and at the end of the simulation. SAM never reaches such conditions due to the higher temperature throughout the troposphere and, hence, a greater saturation mixing ratio. The saturation of the sub-cloud layer in ARPS causes less rain evaporation, weaker downdrafts, and a weaker cold pool effect than those in SAM. Another signal of a weaker cold pool effect is the weaker surface fluxes in ARPS, compared to those in SAM (see Table 2). As shown by (Tompkins, 2001a; Schlemmer & Hohenegger, 2014; Drager & van den Heever, 2017), gusty wind brought by cold pools generally enhance surface fluxes. The weakening of cold pools has been generally proven to favor convective aggregation (Jeevanjee & Romps, 2013; C. Muller & Bony, 2015) through the moisture-memory feedback: moist regions remain moist and thus become more favorable to convection since downdrafts are not able to suppress deep clouds.

550 Moreover, radiative aggregation and the MSE up-gradient circulation are not fa-
 551 vored in ARPS by the smaller amount of shallow clouds (and also a smaller domain frac-
 552 tion covered by downdrafts). On the contrary, the SAM model exhibits a larger amount
 553 of low clouds with a strong radiative cooling at their top (Figure 7). This creates the so-
 554 called “radiatively-driven” cold pools (Coppin & Bony, 2015) and the downdrafts which
 555 initiate the low-level circulation of MSE. Low clouds are sensitive both to domain hor-
 556 izontal resolution and size (C. J. Muller & Held, 2012; C. Muller & Bony, 2015) and also
 557 to the downdrafts strength (Khairoutdinov et al., 2009). Lower resolution and smaller
 558 domain size have been found to decrease the number of shallow clouds in SAM (C. Muller
 559 & Bony, 2015). Such argument was used to explain why self-aggregation does not oc-
 560 cur below a certain resolution and domain size. Khairoutdinov et al. (2009) showed that
 561 removing the evaporation of rain in their simulation (thus weakening cold pools), also
 562 results in a lower shallow cloud fraction covering the domain. In this case, new deep clouds
 563 were found to develop at the sites of previous deep clouds, resembling the moisture-memory
 564 feedback. When rain evaporation was present, deep clouds tended to appear along the
 565 edges of spreading cold pools, favoring also the formation of shallow clouds.

566 Therefore, the convective organization can occur even with a low amount of shal-
 567 low clouds and weak MSE circulation, once it is ensured that the sub-cloud layer is enough
 568 saturated to weaken downdrafts (Wing et al., 2017). Different sub-cloud layer proper-
 569 ties can arise spontaneously from different models even when starting from a similar set-
 570 ting as in the RCEMIP project (Wing et al., 2018). Indeed, Wing et al. (2020) found
 571 a substantial spread in the domain average temperature and humidity profiles after reach-
 572 ing equilibrium.

573 Differences in the way the convective organization is achieved in CRM, by using
 574 other models than SAM, have been noticed in previous studies (Jeevanjee & Romps, 2013;
 575 Yang & Tan, 2020; Tompkins & Semie, 2017; Holloway & Woolnough, 2016). For exam-
 576 ple, Holloway and Woolnough (2016) found that a low level circulation was present in
 577 the Met Office Unified Model, but was driven mainly by anomalies in low-level diabatic
 578 heating from convection and other microphysical processes, and not by radiative cool-
 579 ing gradients between the moist and dry regions. Furthermore, they found that this wasn’t
 580 a crucial organizing feedback. Similarly, this has been found by Yang and Tan (2020)
 581 with WRF. For them, the expansion of dry areas was due to the dry-subsidence feed-
 582 back. Tompkins and Semie (2017), using WRF, found that water vapor feedback with
 583 convection is a necessary but not sufficient condition for convective aggregation. Our work,
 584 as these results, points out that there are still some disagreements between models in
 585 reproducing convective aggregation, as also underlined by (Wing et al., 2020), depend-
 586 ing on their physics and numerics.

587 The ARPS and SAM model reaches their equilibrium in very different ways. We
 588 believe that this is the main reason behind their different final equilibrium state of con-
 589 vective organization. In particular, the small domain simulation of ARPS is entirely cov-
 590 ered by a large anvil (Figure 1) when reaching its equilibrium. Such an anvil blocks in-
 591 coming radiation and the simulation domain starts to get colder and drier with a high
 592 precipitation rate. When initializing the new large simulation, the cloud water and ice
 593 at 12 km are removed, removing the large anvil, while leaving its effect on the vertical
 594 profile of temperature and water vapor. Therefore, an aggregated state is obtained, but
 595 this occurs in a drier and colder domain, with a nearly saturated sub-cloud layer. The
 596 usually adopted procedure of initialization by a small domain (see RCEMIP protocol (Wing
 597 et al., 2018)), is thought to eliminate a long spin-up period to reach the model’s RCE
 598 state without large adjustments (Wing et al., 2018). However, such a procedure could
 599 be affected by the presence of a large optically thin clouds anvil, which will dry and cool
 600 the whole domain. Such presence is evident also in other models of the RCEMIP project,
 601 as shown by large cloud fractions in Figure 9 of Wing et al. (2020).

602 The reason behind the large anvil cloud fraction and cloud ice in the ARPS small
 603 domain simulation has to be found in the microphysics scheme (Lin et al., 1983) and is
 604 closely linked to both the ice aggregation process for snow formation and ice sedimen-

605 tation. Regarding the former process, the threshold for ice aggregation in ARPS is very
 606 high, meaning that in ARPS there is less aggregation of ice to form snow, thus leading
 607 to the presence of more cloud ice. Furthermore, the sedimentation of ice is removed in
 608 ARPS since cloud water and cloud ice are considered to be small enough to have neg-
 609 ligible terminal velocities when compared to rain, snow, and graupel. For these reasons,
 610 in the small domain simulation of the ARPS model, the cloud water/ice covers the en-
 611 tire domain. Instead, in the SAM model, cloud ice is allowed to fall with its own termi-
 612 nal velocity. In Khairoutdinov and Randall (2003) it was verified that the presence of
 613 ice sedimentation in SAM leads to a reduced anvil below 9 km. Thus, in the absence of
 614 ice sedimentation, the anvil in SAM would have been more extensive, than the ARPS
 615 one. As already mentioned in the previous section, the microphysics differences among
 616 the same schemes influence not only the cloud fraction but also the cloud condensate.

617 The updrafts number and velocity are lower in ARPS than in SAM. They could
 618 be diluted by the larger lateral mixing of ARPS (not shown). Following Tompkins and
 619 Semie (2017) greater lateral mixing would help the convective organization. The effect
 620 of mixing will be investigated in more detail in a following paper. However, we note here
 621 that an organized state in SAM is reached with a very small lateral mixing, in contrast
 622 to what was predicted by (Tompkins & Semie, 2017). SAM is likely compensating the
 623 mixing effect with numerical diffusion due to the second-order accurate advection scheme
 624 (Smolarkiewicz & Grabowski, 1990), or the radiative feedback is so strong that aggre-
 625 gation can occur also in an environment where deep convection is not sensitive to en-
 626 trainment (as occurring in the SAM model).

627 5 Conclusions

628 In this study, we performed two RCE simulations with two different CRM (SAM
 629 and ARPS) and we compared their properties while reaching a statistical equilibrium
 630 of precipitation. This study, like other papers using different models besides SAM to in-
 631 vestigate convective organization (Jeevanjee & Romps, 2013; Holloway & Woolnough,
 632 2016; Tompkins & Semie, 2017; Yang & Tan, 2020) point out that there are still some
 633 disagreements between models in reproducing convective aggregation, as also underlined
 634 by (Wing et al., 2020), depending on their physics and numerics.

635 The two models, when reaching the organized state, present a warmer and drier
 636 domain, with a smaller anvil cloud fraction. Similar findings have been obtained in stud-
 637 ies involving idealized 3D simulations (Bretherton et al., 2005; Emanuel et al., 2014; Wing
 638 & Emanuel, 2014), in the RCEMIP project (Wing et al., 2020) and in observations (Tobin
 639 et al., 2012). On the other hand, during the organization, different feedback are at play.
 640 In the SAM model convective organization is achieved due to clouds-radiative feedback
 641 (Stephens et al., 2008; C. J. Muller & Held, 2012; Wing & Cronin, 2016), where the pres-
 642 ence of a deck of low shallow liquid clouds generates a shallow level circulation which trans-
 643 ports MSE up-gradient, making the moist (dry) regions moister (drier). In the ARPS
 644 model, instead, the mechanism behind the onset of the convective organization is that
 645 of moisture-memory feedback (Tompkins, 2001b; Jeevanjee & Romps, 2013; C. Muller
 646 & Bony, 2015), where the convection amplifies in the already moist regions. We found
 647 that, with convective organization, in both models, a warmer atmosphere leads to a re-
 648 duction of the anvil cloud area fraction, the so-called “Iris Effect” (Lindzen et al., 2001;
 649 Mauritsen & Stevens, 2015). Indeed, as mentioned above, in both models the anvil cloud
 650 fraction decreases with the organization.

651 We found that the sub-cloud layer properties are very important for the organi-
 652 zation, because of their relation with downdrafts and cold pools in the RCE simulations,
 653 leading to different feedback between convection and water vapor. This aspect can be
 654 different for different models, even if run in a similar setup, as shown in the RCEMIP
 655 (Wing et al., 2020). Thus it may have important implications for the convective aggre-
 656 gation in models.

We have measured the convective organization in the two models with the same metrics used in RCEMIP. Although a state of the convective organization is reached by both models, their properties are different. We found that SAM and ARPS differ for the final convective cluster dimensions and type and for the degree of organization. The latter is indicated by the value of the Iorg index, higher for the SAM model than for the ARPS model, meaning a stronger organization for the SAM model compared to the ARPS model. Although the RCE average statistics of ARPS, for some aspects (atmospheric energy imbalance and total heat fluxes) are outside the typical range of RCEMIP models; its degree of aggregation corresponds to the average value for the RCEMIP models.

Different degrees of aggregation and different mechanisms bringing to the convective organization, as found in the two models, have different impacts on the climate system. Therefore, theories about climate sensitivity should always consider different types of models, with respect to their physical and numerical formulation.

Open Research

Data Availability Statement

SAM and ARPS models output used in this manuscript are publicly available via Zenodo. The SAM output is available at <https://doi.org/10.5281/zenodo.6949308> and the ARPS output is available at <https://doi.org/10.5281/zenodo.6953873>.

Acknowledgments

This research has been funded by the Italian Ministry of University and Research (MIUR) and University of Perugia within the program *Dipartimenti di Eccellenza 2018-2022*. The authors thank Ming Xue and Marat Khairoutdinov for providing the ARPS and the SAM models, and Kerry Emanuel for the useful discussion during the development of this work.

References

- Bongioannini Cerlini, P., Emanuel, K. A., & Todini, E. (2005). Orographic effects on convective precipitation and space-time rainfall variability: preliminary results. *Hydrology and Earth System Sciences*, *9*(4), 285–299.
- Bretherton, C. S., Blossey, P. N., & Khairoutdinov, M. (2005). An energy-balance analysis of deep convective self-aggregation above uniform SST. *Journal of the atmospheric sciences*, *62*(12), 4273–4292.
- Chou, M.-D. (1990). Parameterizations for the absorption of solar radiation by O_2 and CO_2 with application to climate studies. *Journal of Climate*, *3*(2), 209–217.
- Chou, M.-D., & Suarez, M. J. (1994). An efficient thermal infrared radiation parameterization for use in general circulation models. *NASA Technical Memorandum*, *3*, Article ID 104606.
- Collins, W. D., Rasch, P. J., Boville, B. A., Hack, J. J., McCaa, J. R., Williamson, D. L., . . . Zhang, M. (2006). The formulation and atmospheric simulation of the Community Atmosphere Model version 3 (CAM3). *Journal of Climate*, *19*(11), 2144–2161.
- Coppin, D., & Bony, S. (2015). Physical mechanisms controlling the initiation of convective self-aggregation in a general circulation model. *Journal of Advances in Modeling Earth Systems*, *7*(4), 2060–2078.
- Craig, G. C., & Mack, J. M. (2013). A coarsening model for self-organization of tropical convection. *Journal of Geophysical Research: Atmospheres*, *118*(16), 8761–8769.
- Drager, A. J., & van den Heever, S. C. (2017). Characterizing convective cold pools. *Journal of Advances in Modeling Earth Systems*, *9*(2), 1091–1115.
- Emanuel, K., Wing, A. A., & Vincent, E. M. (2014). Radiative-convective instability. *Journal of Advances in Modeling Earth Systems*, *6*(1), 75–90.
- Hartmann, D. L., & Berry, S. E. (2017). The balanced radiative effect of tropi-

- 708 cal anvil clouds. *Journal of Geophysical Research: Atmospheres*, *122*(9), 5003–
709 5020.
- 710 Held, I. M., Hemler, R. S., & Ramaswamy, V. (1993). Radiative-convective equilib-
711 rium with explicit two-dimensional moist convection. *Journal of Atmospheric*
712 *Sciences*, *50*(23), 3909–3927.
- 713 Hohenegger, C., & Stevens, B. (2016). Coupled radiative convective equilibrium
714 simulations with explicit and parameterized convection. *Journal of Advances*
715 *in Modeling Earth Systems*, *8*(3), 1468–1482.
- 716 Holloway, C. E., & Woolnough, S. J. (2016). The sensitivity of convective ag-
717 gregation to diabatic processes in idealized radiative-convective equilibrium
718 simulations. *Journal of Advances in Modeling Earth Systems*, *8*(1), 166–195.
- 719 Islam, S., Bras, R. L., & Emanuel, K. A. (1993). Predictability of mesoscale rain-
720 fall in the tropics. *Journal of Applied Meteorology and Climatology*, *32*(2),
721 297–310.
- 722 Jeevanjee, N., & Romps, D. M. (2013). Convective self-aggregation, cold pools, and
723 domain size. *Geophysical Research Letters*, *40*(5), 994–998.
- 724 Kessler, E. (1969). On the distribution and continuity of water substance in atmo-
725 spheric circulations. In *On the distribution and continuity of water substance*
726 *in atmospheric circulations* (pp. 1–84). Springer.
- 727 Khairoutdinov, M. F., Blossey, P. N., & Bretherton, C. S. (2022). Global system
728 for atmospheric modeling: Model description and preliminary results. *Journal*
729 *of Advances in Modeling Earth Systems*. (e2021MS002968 2021MS002968) doi:
730 <https://doi.org/10.1029/2021MS002968>
- 731 Khairoutdinov, M. F., & Emanuel, K. (2010). Aggregated convection and the regu-
732 lation of tropical climate. In *29th conf. on hurricanes and tropical meteorology*
733 (pp. P2–69).
- 734 Khairoutdinov, M. F., Krueger, S. K., Moeng, C.-H., Bogenschutz, P. A., & Randall,
735 D. A. (2009). Large-eddy simulation of maritime deep tropical convection.
736 *Journal of Advances in Modeling Earth Systems*, *1*(4).
- 737 Khairoutdinov, M. F., & Randall, D. A. (2003). Cloud resolving modeling of the
738 ARM summer 1997 IOP: Model formulation, results, uncertainties, and sensi-
739 tivities. *Journal of Atmospheric Sciences*, *60*(4), 607–625.
- 740 Lin, Y.-L., Farley, R. D., & Orville, H. D. (1983). Bulk parameterization of the snow
741 field in a cloud model. *Journal of Applied Meteorology and climatology*, *22*(6),
742 1065–1092.
- 743 Lindzen, R. S., Chou, M.-D., & Hou, A. Y. (2001). Does the earth have an adaptive
744 infrared iris? *Bulletin of the American Meteorological Society*, *82*(3), 417–432.
- 745 Liou, K.-N. (1986). Influence of cirrus clouds on weather and climate processes: A
746 global perspective. *Monthly Weather Review*, *114*(6), 1167–1199.
- 747 Mauritsen, T., & Stevens, B. (2015). Missing iris effect as a possible cause of muted
748 hydrological change and high climate sensitivity in models. *Nature Geoscience*,
749 *8*(5), 346–351.
- 750 Muller, C., & Bony, S. (2015). What favors convective aggregation and why? *Geo-*
751 *physical Research Letters*, *42*(13), 5626–5634.
- 752 Muller, C., Yang, D., Craig, G., Cronin, T., Fildier, B., Haerter, J. O., ... others
753 (2022). Spontaneous aggregation of convective storms. *Annual Review of Fluid*
754 *Mechanics*, *54*, 133–157.
- 755 Muller, C. J., & Held, I. M. (2012). Detailed investigation of the self-aggregation
756 of convection in cloud-resolving simulations. *Journal of the Atmospheric Sci-*
757 *ences*, *69*(8), 2551–2565.
- 758 Patrizio, C. R., & Randall, D. A. (2019). Sensitivity of convective self-aggregation
759 to domain size. *Journal of Advances in Modeling Earth Systems*, *11*(7), 1995–
760 2019.
- 761 Pauluis, O., & Held, I. M. (2002a). Entropy budget of an atmosphere in radiative–
762 convective equilibrium. part ii: Latent heat transport and moist processes.

- 763 *Journal of Atmospheric Sciences*, 59(2), 140–149.
- 764 Pauluis, O., & Held, I. M. (2002b). Entropy budget of an atmosphere in radiative–
765 convective equilibrium. part i: Maximum work and frictional dissipation. *Jour-*
766 *nal of the Atmospheric Sciences*, 59(2), 125–139.
- 767 Pope, K. N., Holloway, C. E., Jones, T. R., & Stein, T. H. (2021). Cloud-Radiation
768 Interactions and Their Contributions to Convective Self-Aggregation. *Journal*
769 *of Advances in Modeling Earth Systems*, 13(9), e2021MS002535.
- 770 Randall, D. A., Hu, Q., Xu, K.-M., & Krueger, S. K. (1994). Radiative-convective
771 disequilibrium. *Atmospheric Research*, 31(4), 315–327.
- 772 Robe, F. R., & Emanuel, K. A. (1996). Moist convective scaling: Some inferences
773 from three-dimensional cloud ensemble simulations. *Journal of Atmospheric*
774 *Sciences*, 53(22), 3265–3275.
- 775 Ruppert Jr, J. H., & Hohenegger, C. (2018). Diurnal circulation adjustment and or-
776 ganized deep convection. *Journal of Climate*, 31(12), 4899–4916.
- 777 Schlemmer, L., & Hohenegger, C. (2014). The formation of wider and deeper clouds
778 as a result of cold-pool dynamics. *Journal of the Atmospheric Sciences*, 71(8),
779 2842–2858.
- 780 Schlimme, I., Macke, A., & Reichardt, J. (2005). The impact of ice crystal shapes,
781 size distributions, and spatial structures of cirrus clouds on solar radiative
782 fluxes. *Journal of the Atmospheric Sciences*, 62(7), 2274–2283.
- 783 Semie, A. G., & Bony, S. (2020). Relationship between precipitation extremes
784 and convective organization inferred from satellite observations. *Geophysical*
785 *Research Letters*, 47(9), e2019GL086927.
- 786 Skamarock, W. C., Klemp, J. B., Dudhia, J., Gill, D. O., Barker, D. M., Wang,
787 W., & Powers, J. G. (2005). *A description of the advanced research wrf ver-*
788 *sion 2* (Tech. Rep.). National Center For Atmospheric Research Boulder Co
789 Mesoscale and Microscale .
- 790 Smolarkiewicz, P. K., & Grabowski, W. W. (1990). The multidimensional positive
791 definite advection transport algorithm: Nonoscillatory option. *Journal of Com-*
792 *putational Physics*, 86(2), 355–375.
- 793 Sobel, A. H., Bellon, G., & Bacmeister, J. (2007). Multiple equilibria in a single-
794 column model of the tropical atmosphere. *Geophysical Research Letters*,
795 34(22).
- 796 Stephens, G. L., Van Den Heever, S., & Pakula, L. (2008). Radiative–convective
797 feedbacks in idealized states of radiative–convective equilibrium. *Journal of the*
798 *Atmospheric Sciences*, 65(12), 3899–3916.
- 799 Sun, S., Zhou, B., Xue, M., & Zhu, K. (2021). Scale-similarity subgrid-scale tur-
800 bulence closure for supercell simulations at kilometer-scale resolutions: Com-
801 parison against a large-eddy simulation. *Journal of the Atmospheric Sciences*,
802 78(2), 417–437.
- 803 Tobin, I., Bony, S., & Roca, R. (2012). Observational evidence for relationships be-
804 tween the degree of aggregation of deep convection, water vapor, surface fluxes,
805 and radiation. *Journal of Climate*, 25(20), 6885–6904.
- 806 Tompkins, A. M. (2001a). Organization of tropical convection in low vertical wind
807 shears: The role of cold pools. *Journal of the atmospheric sciences*, 58(13),
808 1650–1672.
- 809 Tompkins, A. M. (2001b). Organization of tropical convection in low vertical wind
810 shears: The role of water vapor. *Journal of the atmospheric sciences*, 58(6),
811 529–545.
- 812 Tompkins, A. M., & Craig, G. C. (1998). Radiative–convective equilibrium in a
813 three-dimensional cloud-ensemble model. *Quarterly Journal of the Royal Mete-*
814 *orological Society*, 124(550), 2073–2097.
- 815 Tompkins, A. M., & Semie, A. G. (2017). Organization of tropical convection in
816 low vertical wind shears: Role of updraft entrainment. *Journal of Advances in*
817 *Modeling Earth Systems*, 9(2), 1046–1068.

- 818 Windmiller, J. M., & Craig, G. C. (2019). Universality in the spatial evolution of
 819 self-aggregation of tropical convection. *Journal of the Atmospheric Sciences*,
 820 *76*(6), 1677–1696.
- 821 Wing, A. A., & Cronin, T. W. (2016). Self-aggregation of convection in long channel
 822 geometry. *Quarterly Journal of the Royal Meteorological Society*, *142*(694), 1–
 823 15.
- 824 Wing, A. A., Emanuel, K., Holloway, C. E., & Muller, C. (2017). Convective self-
 825 aggregation in numerical simulations: A review. *Shallow clouds, water vapor,*
 826 *circulation, and climate sensitivity*, 1–25.
- 827 Wing, A. A., & Emanuel, K. A. (2014). Physical mechanisms controlling self-
 828 aggregation of convection in idealized numerical modeling simulations. *Journal*
 829 *of Advances in Modeling Earth Systems*, *6*(1), 59–74.
- 830 Wing, A. A., Reed, K. A., Satoh, M., Stevens, B., Bony, S., & Ohno, T. (2018).
 831 Radiative–convective equilibrium model intercomparison project. *Geoscientific*
 832 *Model Development*, *11*(2), 793–813.
- 833 Wing, A. A., Stauffer, C. L., Becker, T., Reed, K. A., Ahn, M.-S., Arnold, N. P.,
 834 ... Zhao, M. (2020). Clouds and convective self-aggregation in a multimodel
 835 ensemble of radiative-convective equilibrium simulations. *Journal of Advances*
 836 *in Modeling Earth Systems*, *12*(9), e2020MS002138.
- 837 Xue, M., Droegemeier, K. K., & Wong, V. (2000). The Advanced Regional Predic-
 838 tion System (ARPS)—A multi-scale nonhydrostatic atmospheric simulation and
 839 prediction model. Part I: Model dynamics and verification. *Meteorology and*
 840 *Atmospheric Physics*, *75*(3), 161–193.
- 841 Xue, M., Droegemeier, K. K., Wong, V., Shapiro, A., Brewster, K., Carr, F., ...
 842 Wang, D. (2001). The advanced regional prediction system (arps)—a multi-
 843 scale nonhydrostatic atmospheric simulation and prediction tool. part ii:
 844 Model physics and applications. *Meteorology and atmospheric physics*, *76*(3),
 845 143–165.
- 846 Xue, M., Hu, M., & Schenkman, A. D. (2014). Numerical prediction of the 8 May
 847 2003 Oklahoma City tornadic supercell and embedded tornado using ARPS
 848 with the assimilation of WSR-88D data. *Weather and Forecasting*, *29*(1),
 849 39–62.
- 850 Yang, B., & Tan, Z.-M. (2020). The initiation of dry patches in cloud-resolving con-
 851 vective self-aggregation simulations: Boundary layer dry-subsidence feedback.
 852 *Journal of the Atmospheric Sciences*, *77*(12), 4129–4141.